Accepted Manuscript

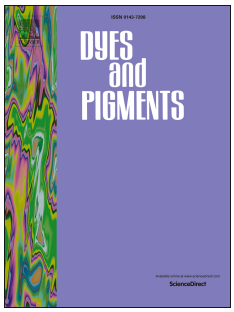

Photophysical properties of acid-responsive triphenylamine derivatives bearing pyridine fragments: Towards white light emission

Jiří Tydlitát, Sylvain Achelle, Julián Rodríguez-López, Oldřich Pytela, Tomáš Mikýsek, Nolwenn Cabon, Françoise Robin-le Guen, David Miklík, Zdeňka Růžičková, Filip Bureš

PII: S0143-7208(17)31213-5

DOI: 10.1016/j.dyepig.2017.07.043

Reference: DYPI 6132

To appear in: *Dyes and Pigments*

Received Date: 25 May 2017

Revised Date: 14 July 2017

Accepted Date: 17 July 2017

Please cite this article as: Tydlitát Jiří, Achelle S, Rodríguez-López Juliá, Pytela Oldř, Mikýsek Tomáš, Cabon N, Robin-le Guen Franç, Miklík D, Růžičková Zdeň, Bureš F, Photophysical properties of acid-responsive triphenylamine derivatives bearing pyridine fragments: Towards white light emission, *Dyes and Pigments* (2017), doi: 10.1016/j.dyepig.2017.07.043.

Photophysical properties of acid-responsive triphenylamine derivatives bearing pyridine fragments: towards white light emission

Jiří Tydlitát,[*,a] Sylvain Achelle,[*,b] Julián Rodríguez-López,[*,c] Oldřich Pytela,[a] Tomáš Mikýsek,[d] Nolwenn Cabon,[b] Françoise Robin-le Guen,[b] David Miklík,[a] Zdeňka Růžičková,[e] and Filip Bureš[a]

[a]Institute of Organic Chemistry and Technology, Faculty of Chemical Technology, University of Pardubice, Studentská 573, Pardubice 53210, Czech Republic. jiri.tydlitat@upce.cz

[b]Institut des Sciences Chimiques de Rennes UMR CNRS 6226, IUT de Lannion, rue Edouard Branly, BP 30219, F22302 Lannion Cedex, France. sylvain.achelle@univ-rennes1.fr

[c]Facultad de Ciencias y Tecnologías Químicas, Universidad de Castilla-La Mancha, 13071 Ciudad Real, Spain. julian.rodriguez@uclm.es

[d]Department of Analytical Chemistry, Faculty of Chemical Technology, University of Pardubice, Studentská 573, Pardubice 53210, Czech Republic.

[e]Department of General and Inorganic Chemistry, University of Pardubice, Studentská 573, Pardubice 53210, Czech Republic

TOC

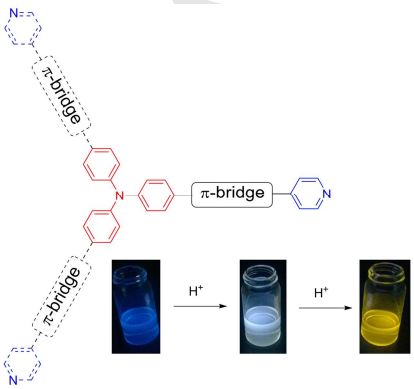

Abstract

The synthesis, thermal, electrochemical, and optical properties of a series of triphenylamine derivatives bearing pyridine fragments and their trifluoroacetate salts are described. A dramatic increase in the intramolecular charge transfer is observed upon protonation, as evidenced by a significant reduction in the HOMO-LUMO gap and a red shift of both the absorption and the emission band. White photoluminescence was obtained in solution by the controlled protonation of blue emitting pyridine derivatives, which resulted in the yellow-orange emissive acidified form. In the solid state the emission color of doped polystyrene thin films could be tuned from steel blue to lawn green when the ratio of the protonated form was increased. These compounds have potential applications in the fabrication of multi-color OLEDs based on only one material.

Keywords: Triphenylamine, Pyridine, Fluorescence, White-light emission, Protonation, Intramolecular charge transfer.

Introduction

In the past decade there has been great interest in the development of white light emitting systems.[1,2] The recent commercialization of White Organic Light Emitting Diodes (WOLEDs), first reported by Kido,[3,4] has been the subject of numerous studies. When compared to their inorganic counterparts, all-organic light emitting molecules have advantages such as lower cost, easy fine tuning of the solution processability, low toxicity, and sufficient flexibility for device fabrication.[2,5–7] White light can be obtained by mixing three primary color emitters (red, green, and blue). Mixing two complementary color emitters in appropriate proportions can also generate white light. White emission was defined by the Commission Internationale d'Eclairage standard colorimetric system (CIE 1931) and it

corresponds to color coordinates close to the Plankian locus around the equi-energy white point (x = 0.33, y = 0.33).[2,8]

White light is generally obtained by the combination of independent chromophores, but a new strategy has recently been proposed that involves the use of two different forms of the same chromophore in equilibrium. The two forms should exhibit complementary emitting colors and can consist of monomer/excimer,[9–11] neutral/(de)protonated species,[12–17] Lewis base/adduct[16] or free/complexed ligand.[18]

Nitrogen-based π-deficient heterocycles such as pyridine,[19–21] pyrimidine,[22–25] pyrazine,[26,27] quinazoline[12,28] or benzimidazole[19,29] can be used as the electron-withdrawing unit in push-pull luminophores. Protonation,[12,22,26,27,30–33] complexation[18,34–36] or alkylation[33,36,37] of such heterocycles enhances their electron-withdrawing character by engaging nitrogen electron lone pairs, thus increasing the intramolecular charge transfer (ICT). This process can lead to emission quenching, but in some cases red shifted emission is observed.[12,22,30–33] Recently, we described white light emission, both in solution and in thin films, from mixtures of neutral and protonated forms of methoxy-substituted pyrimidine derivatives.[38,39]

The triphenylamine (TPA) fragment can be used as a moderate electron-donating unit in push-pull luminophores. Such compounds have been used for their sensing activities *versus* metal cations,[40–42] cyanide,[43–45] water[46] or nitro aromatic explosives.[47–50] The TPA moiety has been extensively used in the design of two photon excited fluorophores,[51–55] mainly for bioimaging applications.[56–59] Moreover, TPA derivatives are known to exhibit aggregation-induced emission properties[46,60,61] and some of these systems have been used in a range of electroluminescent devices.[62–64]

The aim of the work described in this paper was to study the luminescence properties – both in solution and in thin films – of mixtures of neutral and protonated forms of seven TPA

derivatives with pyridine fragments (Chart 1). The results obtained show the potential of these materials in the fabrication of multi-color OLEDs based on only one material.

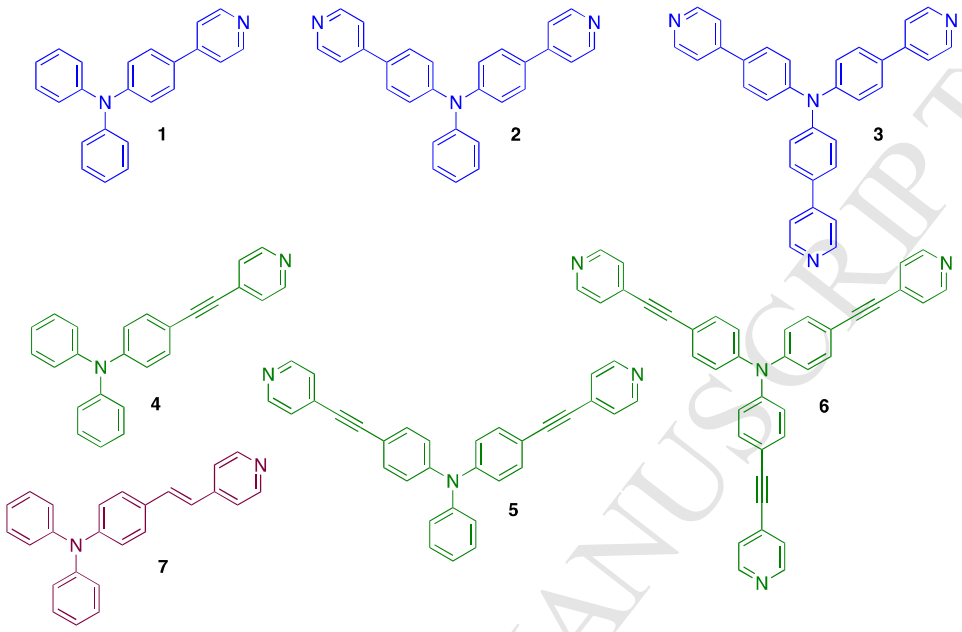

Chart 1.

Results and discussion

Synthesis

Compounds **1**–**3** were obtained in excellent yield by Suzuki cross coupling between pyridin-4-ylboronic acid and the corresponding (poly)iodotriphenylamine according to a literature procedure (Scheme 1).[33] The acetylenic derivatives **4**–**6** were synthesized by Sonogashira cross coupling between 4-iodopyridine and the corresponding (poly)ethynyltriphenylamine. The olefinic derivative **7** was obtained as described in the literature by Heck cross coupling reaction of 4-bromotriphenylamine and 4-vinylpyridine.[65] Trifluoroacetate salts **8**–**14**, i.e., the protonated forms of compounds **1**–**7**, were also isolated. All new materials were characterized by ^{1}H and ^{13}C NMR spectroscopy and by MALDI high-resolution mass spectrometry (MALDI-HRMS).

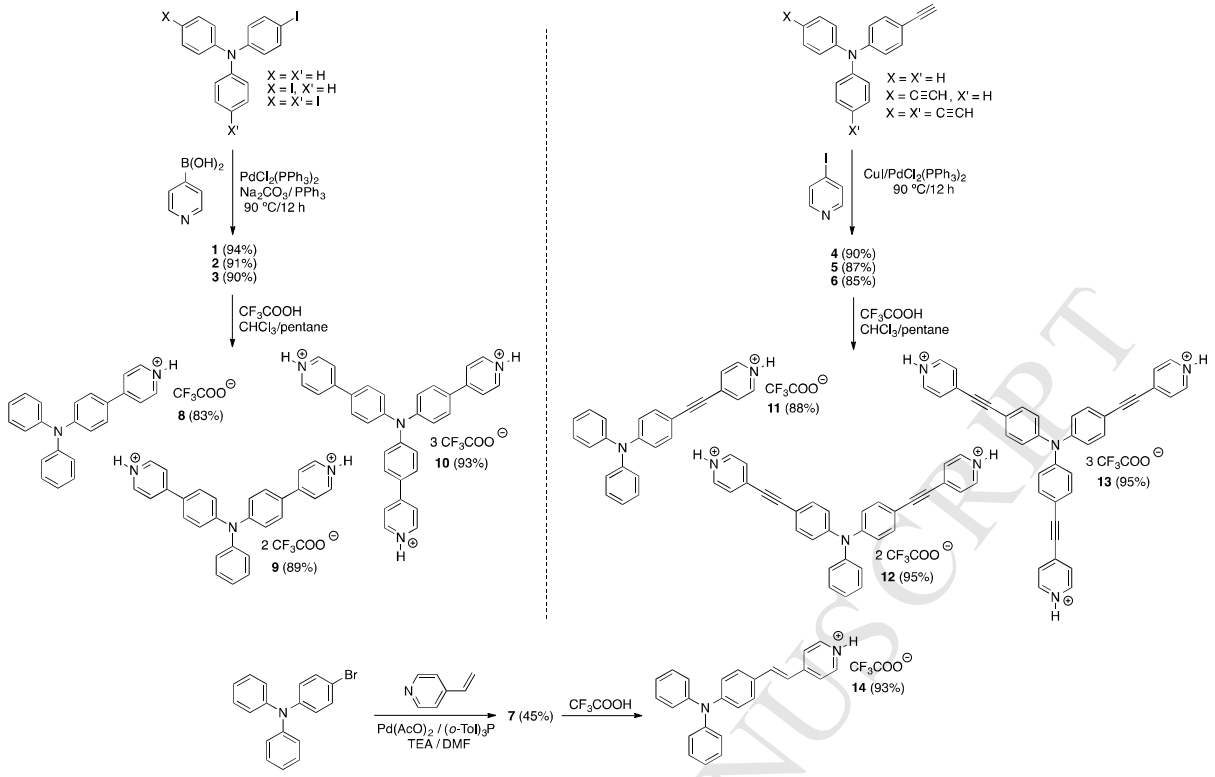

Scheme 1 Synthesis of compounds **1**–**14**.

Single crystal structure

Monocrystals of compounds **1**, **2**, **3** and **10** suitable for X-ray crystal structure analysis were obtained by slow evaporation of the following solvent mixtures $CHCl_3$/EtOAc, EtOAc/EtOH, EtOAc/MeOH, and acetone/$CHCl_3$/pentane, respectively. The ORTEP plots shown in Fig. 1 confirm the proposed molecular structures of **1**, **2**, **3** and **10**. All of these molecules adopt a typical propeller-like arrangement of the central TPA unit. The X-ray structures of **1**, **2**, **3**, and **10** showed a significant twist between the phenyl and pyridine rings with torsion angles of 29–51°. In this respect, the highest value was found for chromophore **1** whereas chromophore **3** showed a lower value for one of its branches, with a torsion angle of 6° enforced by intensive π-stacking between pyridine rings in the crystal (Fig. S43, ESI). Solid state supramolecular assemblies of the chromophores revealed a head-to-tail arrangement typical of dipolar molecules. The X-ray data can further be used to assess the extent of the ICT by

evaluating the aromaticity by considering the Bird index (I_6)[66–68] of the terminal pyridine ring(s). The calculated values for the pyridine rings of **1**, **2** and **3**, and the pyridinium ring of **10** were found to be within the range of I_6 = 93.1–95.9 and 86.7–89.8, respectively. Considering the value of I_6 = 85.7 for unsubstituted pyridine, all terminal pyridine moieties possess relatively high aromatic character – although it is worth noting that this can be reduced by protonation. These findings are consistent with previous values for *N*,*N*-di(pyridin-4-yl)pyridin-4-amine (I_6 = 94.4–95.9).[69]

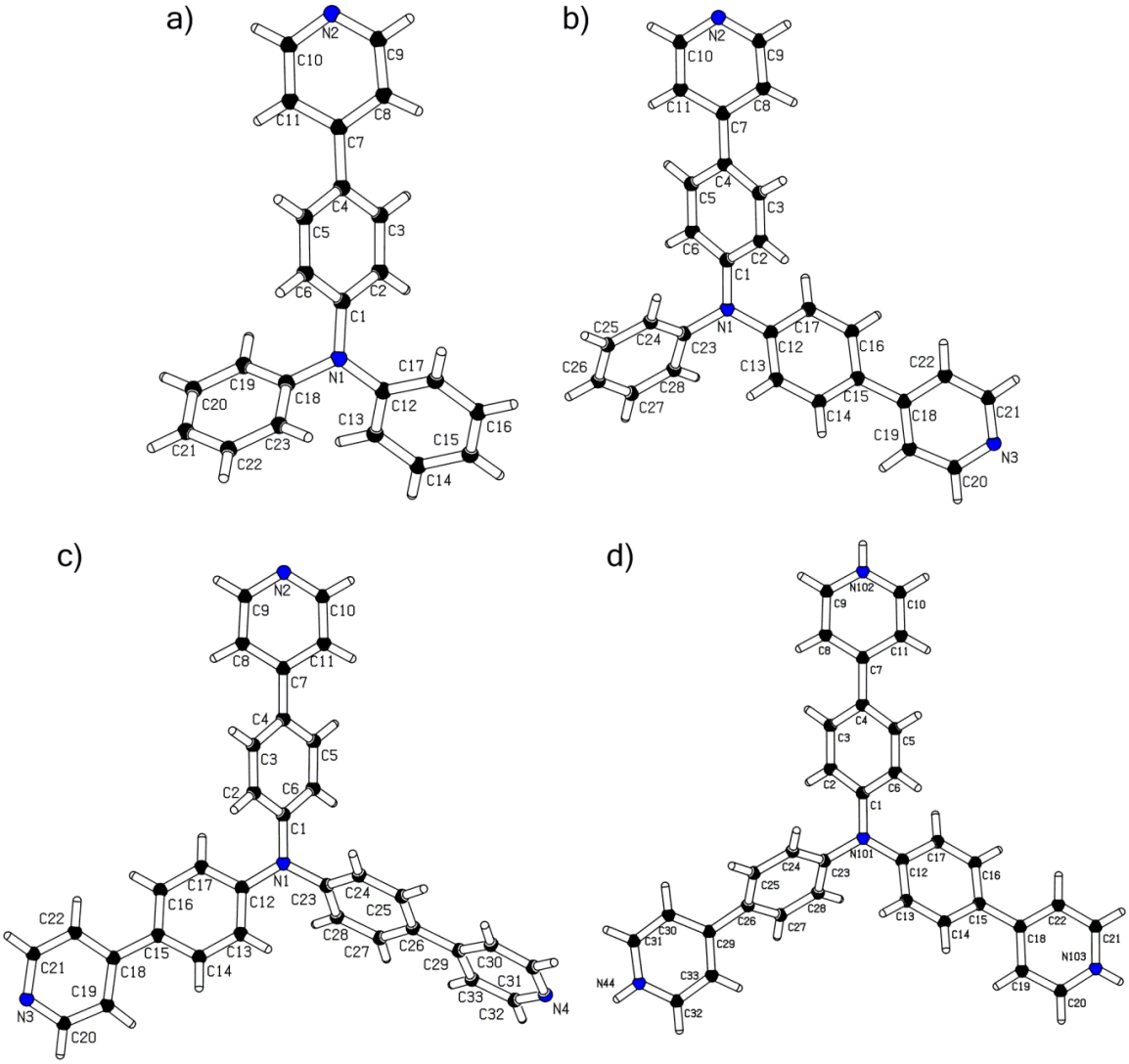

Fig. 1 The molecular structures of a) chromophore **1** (ORTEP 50% probability level), b) chromophore **2** (ORTEP 50% probability level), c) chromophore **3** (ORTEP 50% probability level), and d) pyridinium salt **10** (ORTEP 40% probability level). Solvent molecules and CF_3COO^- ions (for **10**) have been omitted for clarity.

Thermal properties

The thermal behavior of compounds **1**–**14** was studied by differential scanning calorimetry (DSC). Representative thermographs of unprotonated compounds **1**, **5**, and **6** are shown in Fig. 2 and the melting points (T_m) and the thermal decomposition temperatures (T_d) are listed in Table 1. Pyridine-terminated compounds **1**–**7** gave simple and easily interpreted DSC curves. The measured melting points of **1**–**7** range from 118 to 258 °C. The decomposition temperature was estimated to be within the range 248–310 °C. On the other hand, pyridinium salts **8**–**14** exhibited more complicated thermographs with several exo/endothermic processes that were difficult to interpret, probably due to the ionic and multipodal character of the compounds. However, the measured melting points of **8**–**14** range from 115 to 202 °C and the decomposition temperatures were estimated to be within the range 190–220 °C. In general, the pyridinium salts **8**–**14** had lower melting points and lower thermal robustness. For further discussion on the thermal stability of compounds **1**–**14** see the ESI.

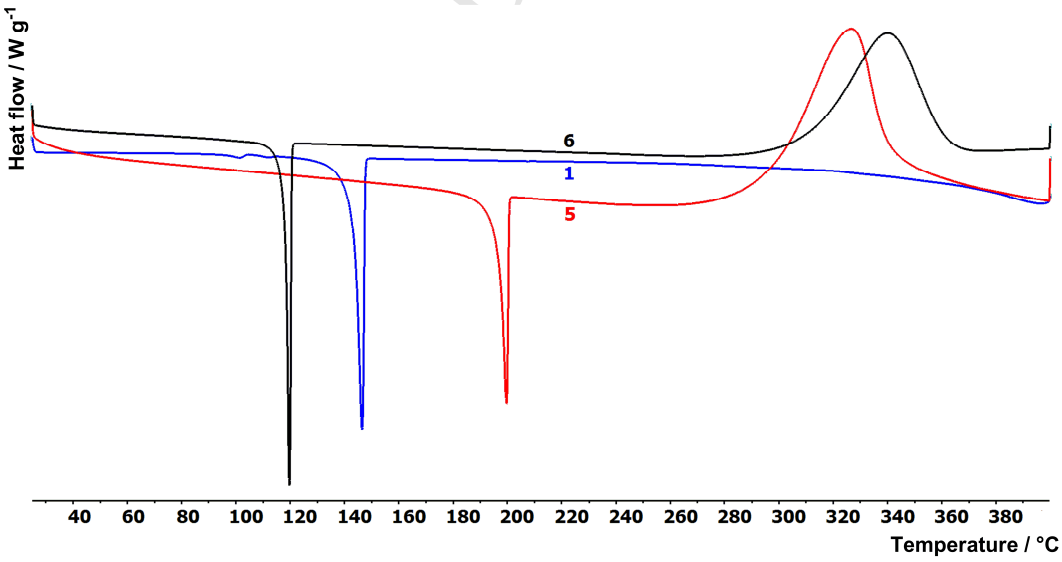

Fig. 2 Representative DSC thermographs of unprotonated compounds **1**, **5** and **6** obtained with a scanning rate of 3 °C/min in the range 25–400 °C.

Table 1 Thermal and electrochemical properties of chromophores **1**–**14**.

Compd	T_m[a] (°C)	T_d[b] (°C)	$E_{1/2}^{(ox1)}$[c,d] (V)	$E_{1/2}^{(red1)}$[c,e] (V)	ΔE[c] (V)	E_{HOMO}[f] (eV)	E_{LUMO}[f] (eV)
1	143	/	1.07	–2.15	3.22	–5.42	–2.20
2	147	≈248	1.09	–2.10	3.19	–5.44	–2.25
3	258	/	1.11	–2.07	3.17	–5.46	–2.28
4	196	295	1.09	–1.96	3.05	–5.44	–2.40
5	118	310	1.12	–1.86	2.98	–5.47	–2.49
6	235	256	1.19	–1.85	3.04	–5.54	–2.50
7	/	286	1.06	–1.82	2.87	–5.41	–2.54
8	115	200	1.12	–1.21	2.33	–5.47	–3.14
9	133	220	1.13	–1.19	2.32	–5.48	–3.16
10	196	207	1.14	–1.17	2.32	–5.49	–3.18
11	141	190	1.07	–1.07	2.14	–5.42	–3.28
12	/	192	1.11	–1.05	2.16	–5.46	–3.30
13	/	199	1.15	–1.02	2.17	–5.50	–3.33
14	189	201	0.96	–1.00	1.96	–5.31	–3.35

[a] T_m = melting point (the point of intersection of a baseline before the thermal effect with a tangent). [b] T_d = thermal decomposition (pyrolysis in a N_2 atmosphere). [c] $E_{1/2}^{(ox1)}$ and $E_{1/2}^{(red1)}$ are half-wave potentials of the first oxidation and reduction, respectively; all potentials are given *vs* SCE (Saturated Calomel Electrode); $\Delta E = E_{1/2}^{(ox1)} - E_{1/2}^{(red1)}$. [d] Pt disk – RDV [e] Hg drop– polarography [f] $E_{HOMO/LUMO} = E_{1/2}^{(ox1/red1)} + 4.35$.

Electrochemistry

Electrochemical measurements on chromophores **1**–**14** were carried out in DMF containing 0.1 M Bu_4NPF_6 in a three electrode cell by cyclic voltammetry (CV), rotating disc voltammetry (RDV), and polarography.

The measured half-wave potentials of the first oxidation and reduction ($E_{1/2}^{(ox1)}$ and $E_{1/2}^{(red1)}$) of chromophores **1**–**14**, measured by RDV and polarography experiments respectively, were found within the ranges 0.96 to 1.19 and –1.00 to –2.15 V *vs* SCE, respectively. The first reduction and oxidation are followed by subsequent oxidations and reductions, and they are clearly a function of the peripheral acceptor and the π-linker (Table 1). Whereas the first one electron oxidation can be attributed to the central TPA donor, the first reduction is mostly localized on the terminal pyridine/pyridinium ring and the appropriate π-linker. The LUMO and HOMO energy levels (easily calculated from the first oxidation and reduction potentials as $-E_{LUMO/LUMO} = E_{1/2}^{(red1)/(ox1)} + 4.35$) of chromophores **1**–**14** can be discussed from two

points of view involving the branching and the nature of the π-linker. On changing from linear across quadrupodal to tripodal derivatives, a general decrease in the LUMO energies is observed for both pyridine and pyridinium derivatives. The most obvious difference was seen for acetylenic pyridine derivatives **4** and **6** with E_{LUMO} = –2.40 and –2.50 eV, respectively. The HOMO energy levels showed similar trends. Within the series of linear derivatives **1**, **4**, and **7**, which incorporate various π-linkers, E_{LUMO} decreases from –2.20 eV for chromophore **1** to –2.54 eV for olefinic derivative **7**. Linear pyridinium derivatives **8**, **11**, and **14** generally possess lower energies than the corresponding pyridine-terminated derivatives **1**, **4**, and **7** due to higher electron-withdrawing power of the pyridinium over pyridine moieties. On the other hand, E_{HOMO} increases within the same series of compounds with the highest values of –5.41 and –5.31 eV obtained for pyridine **7** and pyridinium **14**, both of which are olefinic derivatives. In any case, the best way to evaluate the impact of the structural features on the electrochemical properties is through the HOMO-LUMO gap Δ*E*. The parallel trends outlined above for the HOMO and LUMO energies imply that branching did not affect the Δ*E* absolute values but rather shifts in both HOMO and LUMO levels to lower values occur. This situation is consistent with our recent general observation on branching.[70] The effect of the π-linker can be demonstrated in series **1** (none), **4** (acetylenic) and **7** (olefinic) or **8** (none), **11** (acetylenic) and **14** (olefinic). In both series there is a steady decrease in Δ*E* caused mostly by variation of the E_{LUMO} (see Fig. 3). This energy level diagram further illustrates differences between pyridine- and pyridinium-terminated chromophores. The latter showed decreases in the HOMO-LUMO gap by 0.89–0.91 eV. The smallest HOMO-LUMO gap of 1.96 eV was measured for linear pyridinium chromophore **14**. When comparing these results with those of previous tripodal TPA derivatives bearing 4-cyanophenyl acceptors,[71] pyridine analogs showed higher Δ*E* values by 0.16–0.22 eV, whereas pyridinium derivatives have Δ*E* values that are significantly narrowed by 0.69–0.75 eV.

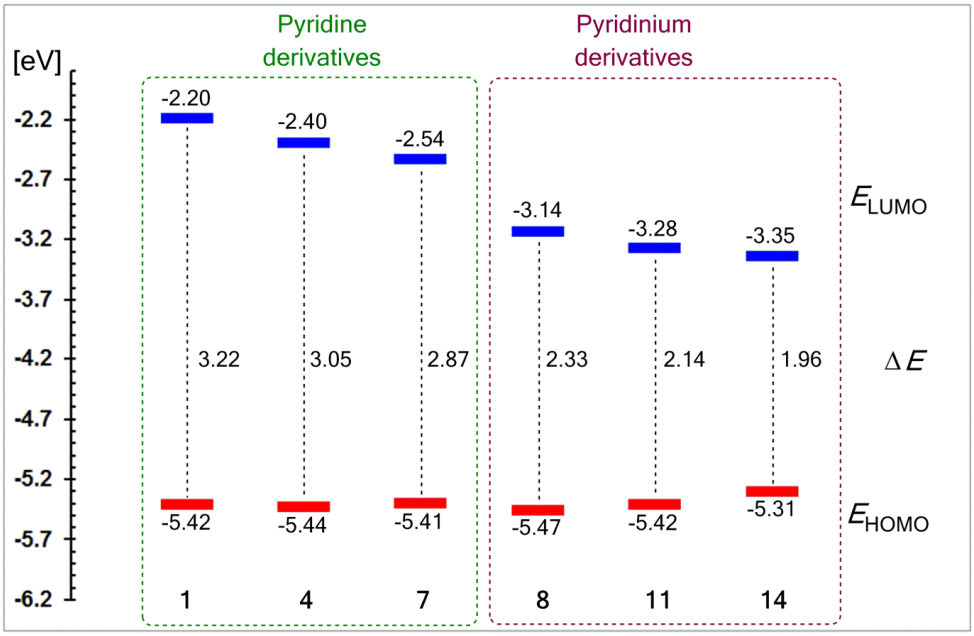

Fig. 3 Energy level diagram for linear chromophores **1**, **4**, **7**, **8**, **11**, and **14**.

DFT calculations

The spatial and electronic properties of chromophores **1**–**14** were investigated using the Gaussian W09 package[72] at the DFT level. The initial geometries of molecules **1**–**14** were estimated and optimized using the DFT B3LYP/6-31G(d) and DFT B3LYP/6-311G(2d,p) methods. The HOMO and LUMO energies, their differences, and the ground state dipole moments were calculated at the DFT B3LYP/6-311++G(2d,p) level and are summarized in Table 2.

Table 2 DFT calculated properties of chromophores **1**–**14**.

Compd	Symmetry group	E_{HOMO}[a] (eV)	E_{LUMO}[a] (eV)	ΔE (eV)	μ (D)
1	C2	–5.44	–1.57	3.88	3.8
2	C2	–5.57	–1.80	3.77	3.6
3	D3	–5.69	–1.92	3.77	0.0
4	C2	–5.45	–1.94	3.51	5.0
5	C2	–5.58	–2.22	3.36	4.4
6	D3	–5.68	–2.34	3.34	0.0
7	C1	–5.36	–2.05	3.30	4.8
8	C2	–8.32	–5.78	2.54	13.9
9	C2	–10.46	–8.01	2.45	11.6
10	D3	–12.34	–9.52	2.82	0.0
11	C2	–8.01	–5.88	2.12	17.4
12	C2	–9.78	–7.66	2.12	14.4
13	C3	–11.31	–8.94	2.37	0.1
14	C1	–7.97	–5.75	2.22	16.2

[a]Calculated at the DFT B3LYP/6-311++G(2d,p) level.

The calculated energies of the HOMO of pyridine derivatives **1**–**7** range from –5.69 to –5.36 eV and the LUMO energies from –2.34 to –1.57 eV and these values reflect structural differences of the individual chromophores. In contrast to the electrochemical measurements, the calculated energies of **8**–**14** are affected by anion exclusion and by calculation in vacuum. Hence, generally higher HOMO and LUMO values of –7.97 to –12.34 eV and –5.75 to –9.52 eV were obtained. However, the calculated *ΔE* values correlate reasonably well with the experimental values obtained by electrochemical measurements (Fig. S44, ESI). Comparison with the electrochemical data shows similar trends in the calculated HOMO and LUMO energies, i.e., branching, π-linker nature and electron-withdrawing power of pyridine and pyridinium moieties affect the Δ*E* most significantly. The calculated HOMO-LUMO gaps, which were within the range 3.88–2.12 eV, correlate well with the electrochemical data, with differences between 0.02 and 0.66 eV. The HOMO and LUMO localizations in representative molecules (for a complete listing see the ESI) are shown in Fig. 4. As expected, the HOMO is localized on the central TPA donor, whereas the LUMO is predominantly spread over the

pyridine or pyridinium acceptors. In quadrupolar and tripodal molecules, the LUMO occupies mostly one or two branches and the third one is occupied by the LUMO+1. This is a common feature of multipodal push-pull chromophores.[70,71] The calculated ground state dipole moments strictly obey the molecular structure of the particular chromophores. While tripodal molecules **3**, **6**, and **10** with D3 symmetry have almost zero dipole moment, the remaining ones that fall within the C1, C2 and C3 symmetry groups had dipole moments within the range 0.1–17.4 D.

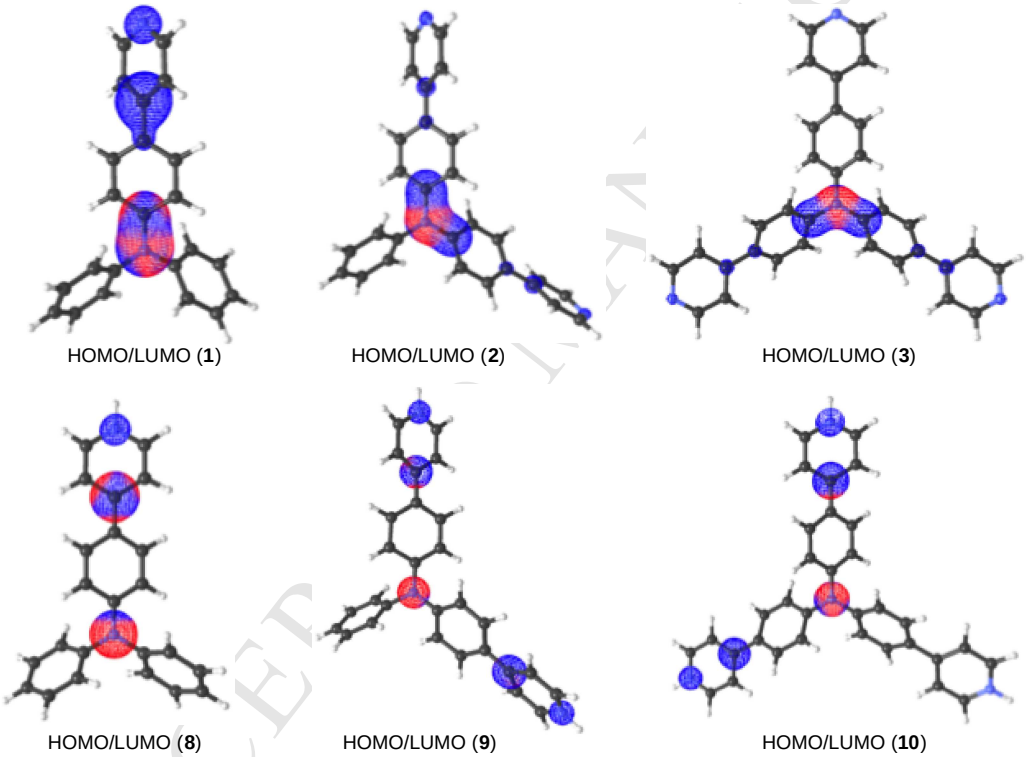

Fig. 4 Representative HOMO (red) and LUMO (blue) localizations in **1**–**3** and **8**–**10**.

UV-vis and fluorescence spectroscopy

The UV-vis and photoluminescence (PL) spectroscopic data for compounds **1**–**7**, measured in chloroform, are presented in Table 3. The analyses were carried out using low concentration solutions ((1.0–2.0) × 10^{-5} M). Under these conditions, self-absorption effects were not observed. As representative examples, the spectra of derivatives **4**–**6** are shown in Fig. 5.

Table 3 UV-vis and photoluminescence (PL) data in $CHCl_3$ solution.

Compd	λ_{abs} (nm)	ε (mM^{-1} cm^{-1})	λ_{em} (nm)	Φ_F[a]	Stokes shift (cm^{-1})	Brightness[b] (mM^{-1} cm^{-1})
1	349	25.6	444	0.50	6130	12.8
2	363	26.5	431	0.54	4346	14.3
3	361	55.4	429	0.50	4391	27.7
4	292, 370	14.6, 31.0	456	0.78	5097	24.1
5	258, 382	27.4, 44.2	442	0.74	3347	32.7
6	271, 382	43.0, 76.6	439	0.63	3347	48.2
7	296, 386	19.6, 28.0	485	0.45	5288	12.6

[a]Fluorescence quantum yield (±10%) determined relative to 9,10-bis(phenylethynyl)anthracene in cyclohexane (Φ_F = 1.00) as standard. [b]Calculated as the product of ε and Φ_F.

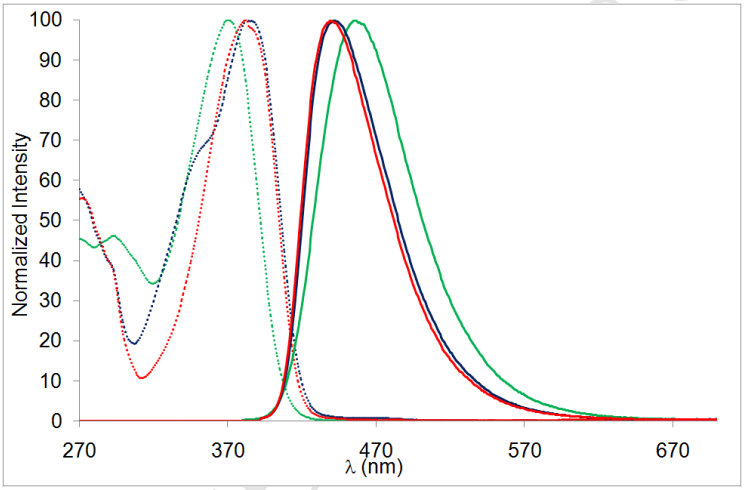

Fig. 5 Normalized absorption (dashed lines) and emission spectra (solid lines) of compounds **4** (green), **5** (blue), and **6** (red) in $CHCl_3$ solution.

All of the compounds exhibited intense blue luminescence with fluorescence quantum yields (Φ_F) up to 78%. A bathochromic shift of the charge transfer absorption band was observed on going from a mono-substituted (dipolar) to a di- or tri-substituted (quadrupolar or octupolar) TPA, while the emission band was hypsochromically shifted. This effect leads to a decreased Stokes shift and is consistent with results obtained for similar TPA derivatives.[51,73] For octupolar TPA derivatives, a dramatic increase in the molar extinction coefficient and brightness was found. This feature is ascribed to the degeneracy of the S1 state of these compounds, which alters the electronic levels of the TPA core through π-conjugation.[73] When

comparing the three monosubstituted TPA derivatives (compounds **1**, **4**, and **7**), the absorption and emission maxima increase in the order λ_{max} (**1**) < λ_{max} (**4**) < λ_{max} (**7**), thus indicating an enhanced ICT when a π-linker is placed between the TPA fragment and the pyridine moiety, in accordance with electrochemical measurements. This observation is also consistent with results reported for related compounds.[51]

Solvatochromic behavior

The solvatochromic shifts of the emission bands can be used to evaluate the ICT upon excitation into push-pull compounds. With such compounds a broad, structureless red-shifted emission is observed on increasing the solvent polarity along with a successive decrease of the fluorescence intensity. This positive solvatochromic behavior, which results from the stabilization of a highly polar emitting state by polar solvents, has been fully documented for donor-acceptor fluorophores.[22,26,27,52,56–59] Thus, the emission spectra of the studied compounds were measured in seven aprotic solvents of different polarity. The results of these investigations are summarized in Table 4. For all compounds, a bathochromic shift of the emission band was observed as the solvent polarity was increased, as predicted by the Dimroth–Reichardt polarity parameters ($E_T(30)$).[74,75] As examples, the changes in the emission spectra of **4** and in the color of a solution of **7** under UV irradiation in various solvents are shown in Figs. 6 and 7, respectively. Good linearity was observed when the emission maxima were plotted *vs* $E_T(30)$ in all cases (Fig. 8). The slopes of the corresponding regression lines are good indicators of the intensity of the ICT. Concerning monosubstituted dipolar TPA derivatives, in accordance with the observations on the position of absorption and emission maxima, the slope increased when acetylenic or olefinic linkers were added (**4** and **7** *vs* **1**). Surprisingly, the slope is higher for **4** than for **7**. Increasing the substitution of the TPA core decreased the value of the slope.

Table 4 Emission solvatochromism of TPA derivatives **1**–**7** in various aprotic solvents.

	Heptane	Toluene	THF	CH_2Cl_2	Acetone	MeCN	DMSO
	30.9[a]	33.9[a]	37.4[a]	40.7[a]	42.2[a]	45.6[a]	45.1[a]
Compd	λ_{max} (nm)	λ_{max} (nm)	λ_{max} (nm)	λ_{max} (nm)	λ_{max} (nm)	λ_{max} (nm)	λ_{max} (nm)
1	389	412	433	451	458	472	472
2	394	407	428	442	449	467	463
3	390	408	427	441	449	460	461
4	398	421	450	473	481	497	506
5	404	419	435	453	466	480	493
6	404	416	437	451	465	477	483
7	424	448	475	498	500	515	521

[a] $E_T(30)$, Dimroth–Reichardt polarity parameter in kcal mol^{-1}.

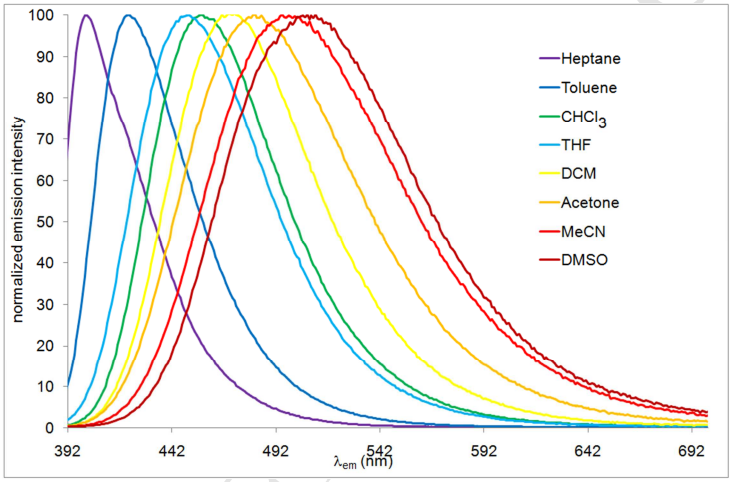

Fig. 6 Normalized emission spectra of **4** in different aprotic solvents.

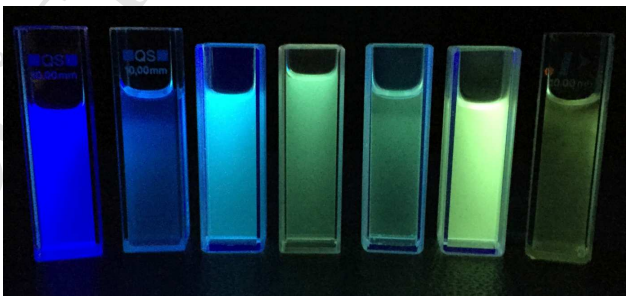

Fig. 7 Fluorescence color changes experienced by **7** in various solvents (from left to right: heptane, toluene, THF, CH_2Cl_2, acetone, MeCN, DMSO). Picture was taken in the dark upon irradiation with a hand-held UV lamp (λ_{em} = 366 nm).

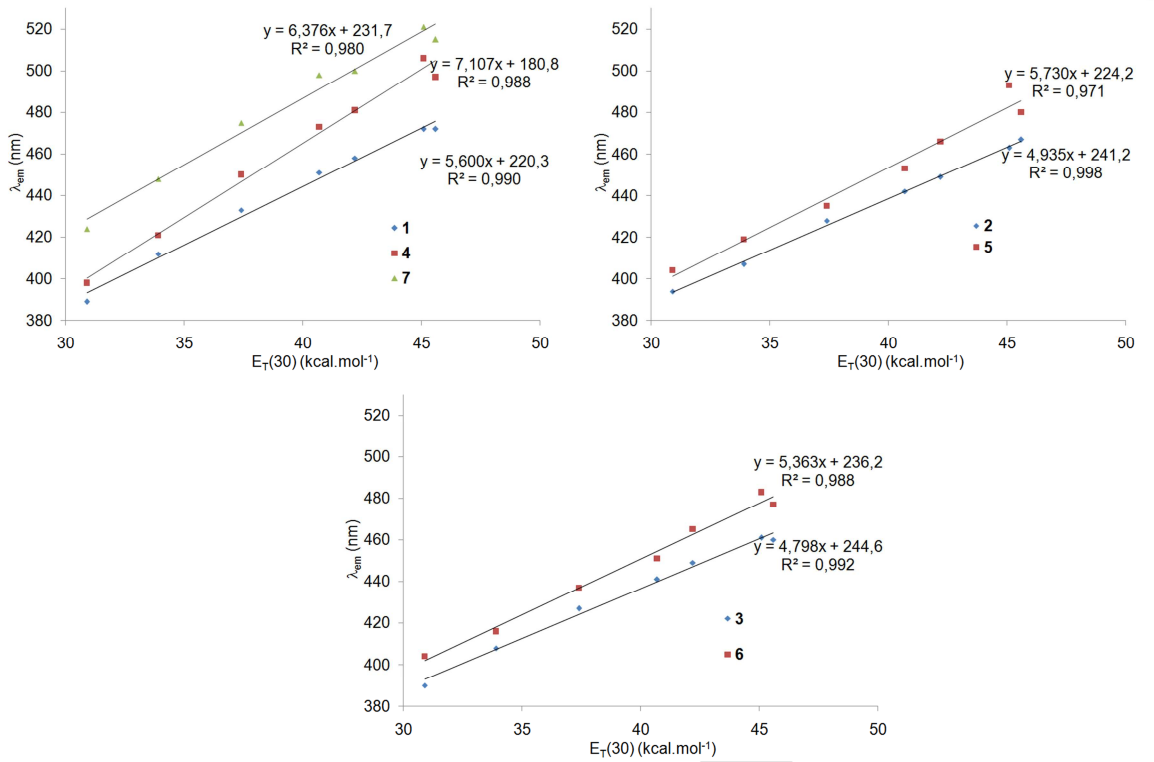

Fig. 8 Emission maxima (λ_{em}) as a function of the Dimroth–Reichardt polarity parameter $E_T(30)$ for TPA derivatives **1**–**7**.

Protonation study

NMR studies. Protonation of the pyridine-terminated chromophore **4** was studied by ^{1}H NMR spectroscopy (Fig. 9). The gradual addition of trifluoroacetic acid (TFA) to a $CDCl_3$ solution of **4** resulted in the shift of particular signals, especially those belonging to the pyridine ring. Initially, the ^{1}H NMR spectrum of **4** showed two sets of doublets (H^A/H^B and H^C/H^D) corresponding to the pyridine and the 1,4-phenylene units, respectively, as well as three additional groups of signals ($H^E/H^F/H^G$) for the additional two phenyl rings.

Upon addition of TFA, the pyridine signals H^A/H^B were progressively shifted downfield. As expected, the positions of the remaining signals were affected to a lesser extent by protonation. The absence of two sets of signals for mixtures of **4** and **11** (e.g., green, violet, and yellow spectra) indicates a fast proton exchange in solution. Protons H^B showed the largest difference in the chemical shifts (7.33 ppm in **4** *vs* 7.71 ppm in **11**). The coupling

constant $^{3}J(H^{A},H^{B})$ also increased upon protonation (5.3 Hz in **4** *vs* 6.0 Hz in **11**). The upper-most red spectrum corresponds to a 1:1 mixture of **4** and TFA, and is in full accordance with the spectrum obtained for the pyridinium salt **11** (see the Experimental section).

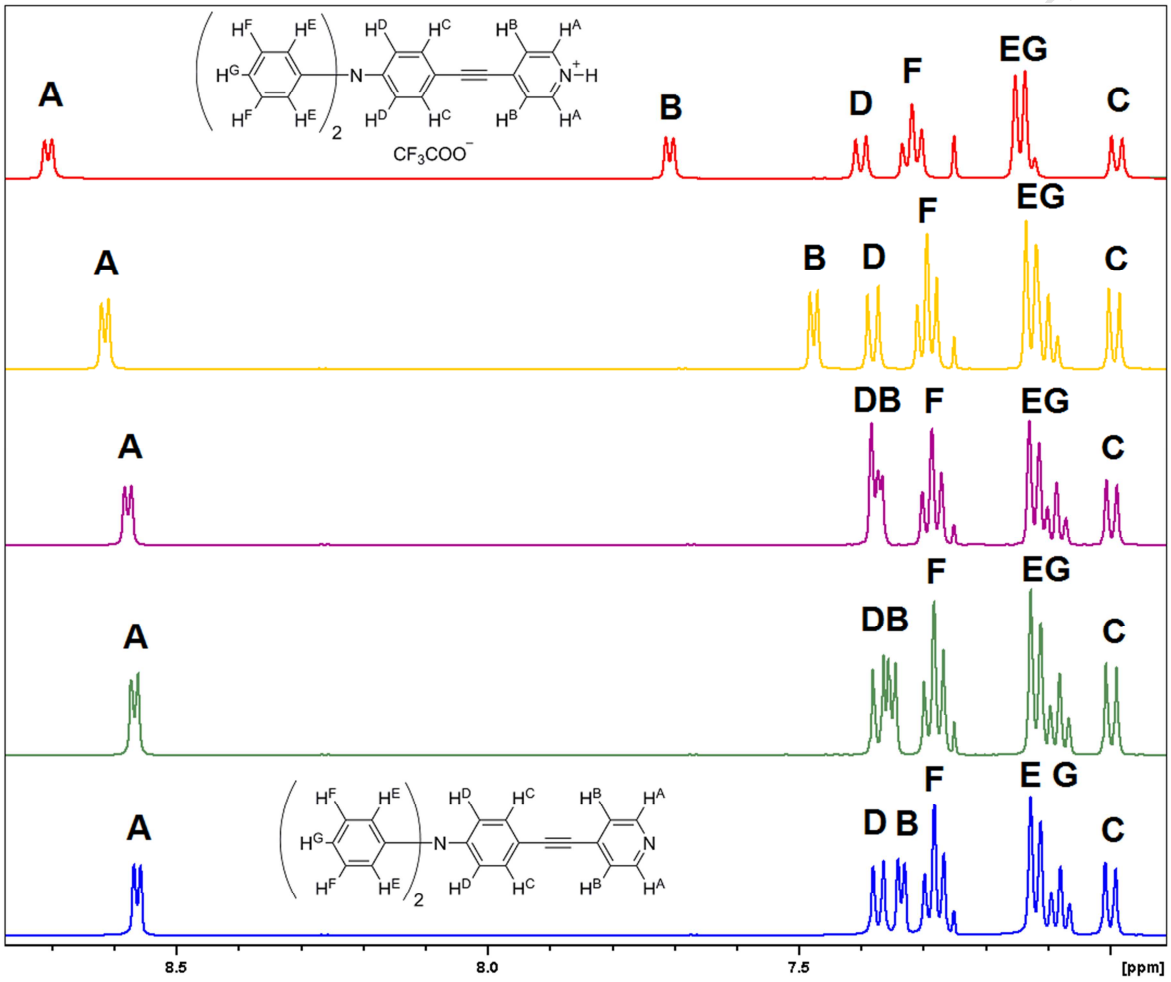

Fig. 9 ^{1}H NMR protonation study on chromophore **4** by gradual addition of TFA. The blue trace corresponds to the pyridine derivative **4** while the red trace corresponds to the pyridinium derivative **11**.

Photophysical properties in solution. Photophysical measurements were also performed in acid solution (10^{-2} M TFA in $CDCl_3$) for compounds **1**–**7**. The results are summarized in Table 5. As expected, a bathochromic shift in the absorption and emission bands was observed upon protonation. In general, this shift was accompanied by a decrease in both the

fluorescence quantum yield and brightness, although these values remained relatively high for octupolar chromophores **3** and **6**. An emission solvatochromic study was also performed for compound **8** (Fig. 10). In this case, it is worth noting that the emission was almost totally quenched for the more polar solvents (acetone, MeCN and DMSO). The slope of the regression lines of the emission maxima *vs* polarity parameters increased dramatically after acidification of the solvent (Fig. 10B, 9.70 nm.mol.kJ^{-1} *vs* 5.60 nm.mol.kJ^{-1}) and this is consistent with a significant enhancement of the ICT into the fluorophore after protonation.

Table 5 UV/vis and PL data in acid solution (10^{-2} M TFA in $CHCl_3$).

Compd	λ_{abs} (nm)	ε (mM^{-1} cm^{-1})	λ_{em} (nm)	Φ_F[a]	Stokes shift (cm^{-1})	Brightness[b] (mM^{-1} cm^{-1})
8	416	28.9	584	0.15	6915	4.3
9	430	35.6	540	0.42	4737	14.9
10	417	53.4	521	0.48	4787	25.6
11	449	31.0	623	0.05	6220	1.55
12	452	42.3	594	0.18	5288	7.6
13	442	60.7	579	0.31	5353	18.8
14	467	27.5	612	0.24	5073	6.6

[a]Fluorescence quantum yield (±10%) determined relative to 9,10-bis(phenylethynyl)anthracene in cyclohexane (Φ_F = 1.00) as standard. [b]Calculated as the product of ε and Φ_F.

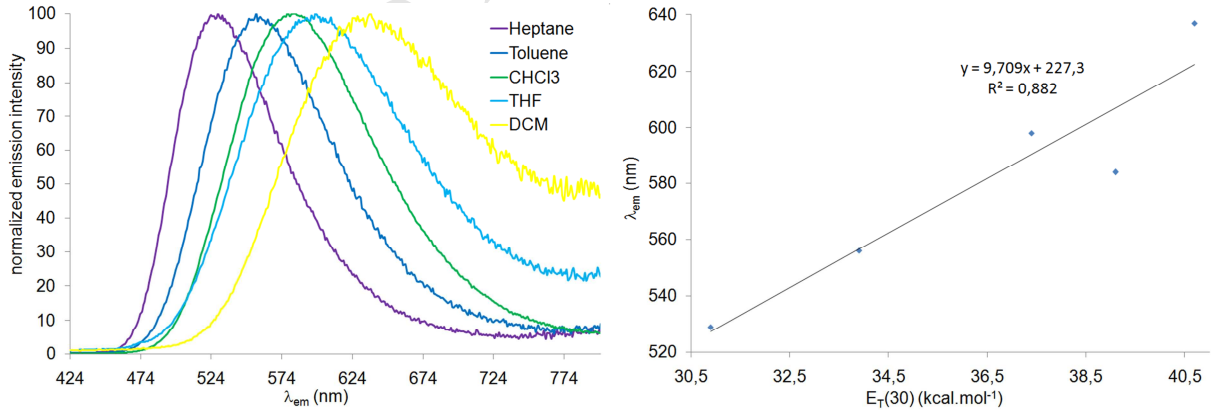

Fig. 10 A) Normalized emission spectra of **8** in different aprotic solvents. B) Emission maxima (λ_{em}) as a function of the Dimroth–Reichardt polarity parameters.

For all of the TPA chromophores, the effect of protonation in chloroform solution was studied by titration with TFA. As an example, the changes observed in the UV-vis and emission spectra of **7** upon the addition of acid are illustrated in Figs. 11 and 12, respectively (Fig. S51–S61 for the spectra of compounds **1**–**6**, ESI). The absorption spectra showed the progressive attenuation of the charge transfer absorption band for the neutral compounds on increasing the concentration of acid, whereas a new red-shifted band corresponding to the protonated species appeared. Isosbestic points were observed for TPA derivatives **1**, **4**, and **7**, which bear only one pyridine ring. This is not the case for the other derivatives due to the coexistence of diprotonated or triprotonated species. Surprisingly, compounds with acetylenic linkers (**4**–**6**) required a significantly higher TFA concentration before changes in their absorption spectra were observed. The same trends were observed in the emission properties, i.e., the addition of TFA led to a decrease in the emission band intensity and a new red-shifted band appeared with an isoemissive point for monosubstituted TPA derivatives. The intensity of both bands became similar after the addition of 0.8 equiv of TFA to a solution of **7** in $CHCl_3$ (λ_{exc} = 410 nm) (Fig. 12). The coexistence of both neutral and protonated forms led this solution to emit white light under UV irradiation, while under the same conditions, the nonprotonated and fully protonated solutions appeared blue and orange, respectively (Fig. 13). Similar behavior was observed for compounds **1**–**6** and chromaticity coordinates close to those of pure white light (0.33, 0.33) could be obtained in all cases (Table 6). It is noteworthy that in the case of compound **4** the addition of TFA resulted in a dramatic decrease in the emission intensity. Thus, low emission intensity was observed when both bands reached the same height (Fig. S59, ESI).

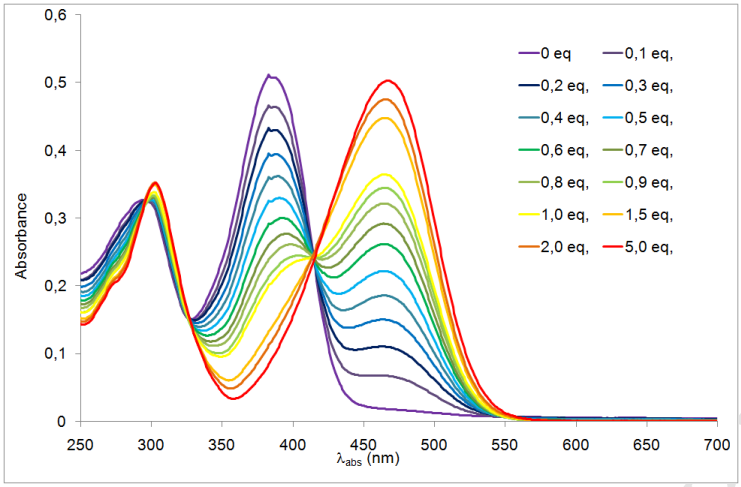

Fig. 11 Changes in the absorption spectra of a $CHCl_3$ solution of **7** (c = 1.86 × 10^{-5} M) upon addition of TFA (0.1–5.0 equiv).

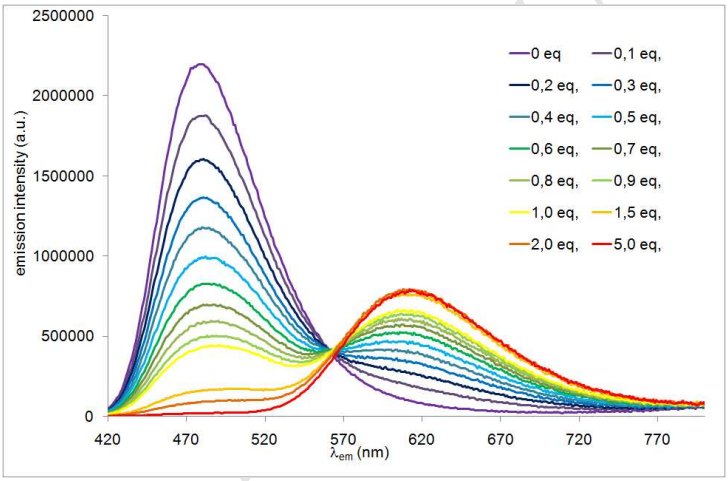

Fig. 12 Changes in the emission spectra of a $CHCl_3$ solution of **7** (c = 1.86 × 10^{-5} M) upon addition of TFA (0.1–5.0 equiv). λ_{exc} = 410 nm.

Fig. 13 Changes in the color of a $CHCl_3$ solution of **7** (c = 1.86 × 10^{-5} M) after the addition of 0.8 equiv (middle) and 5 equiv of TFA (right). Photographs were taken in the dark upon irradiation with a hand-held UV lamp (λ_{em} = 366 nm).

Table 6 CIE coordinates for TPA derivatives in $CHCl_3$ solution (c = (1.0–2.0) × 10^{-5} M).

	Chromaticity coordinates (x,y)		
Compd	Neutral form	Protonated form	Mixture of neutral and protonated forms
1	(0.17, 0.12)	(0.45, 0.47)	(0.33, 0.32)[a]
2	(0.16, 0.08)	(0.38, 0.56)	(0.33, 0.35)[b]
3	(0.16, 0.07)	(0.35, 0.51)	(0.30, 0.34)[c]
4	(0.15, 0.16)	(0.45, 0.39)	(0.34, 0.30)[d]
5	(0.15, 0.10)	(0.45, 0.40)	(0.35, 0.31)[e]
6	(0.15, 0.09)	(0.51, 0.45)	(0.34, 0.30)[f]
7	(0.17, 0.29)	(0.51, 0.49)	(0.32, 0.36)[g]

[a] 0.8 equiv of TFA, λ_{exc} = 380 nm. [b] 4.0 equiv of TFA, λ_{exc} = 390 nm. [c] 10.0 equiv of TFA, λ_{exc} = 380 nm. [d] 400 equiv of TFA, λ_{exc} = 390 nm. [e] 250 equiv of TFA, λ_{exc} = 250 nm. [f] 160 equiv of TFA, λ_{exc} = 390 nm. [g] 0.6 equiv of TFA, λ_{exc} = 410 nm.

Photophysical properties in thin film. According to the protocol that some of us described previously for a pyrimidine fluorophore,[38] thin films of polystyrene doped with 1 wt% of compounds **1** and **7** were prepared using different ratios of neutral and protonated forms. The emission spectra of the samples obtained for **1** are shown in Fig. 14. Although the films remained luminescent, both bands experienced a significant blue shift when compared to the $CHCl_3$ solution. In this case, the chromaticity coordinates were far from those of pure white light regardless of the neutral (**1**)/protonated (**8**) form ratio (Table 7). When compound **7** was used, it was not possible to obtain white luminescence either, although the chromaticity coordinates were closest to those of white light when 0.6 equiv of TFA were employed (0.25, 0.36) (Table S4, ESI). Nevertheless, with this fluorophore the emission color of the thin film could be tuned from steel blue to lawn green through cyan when the ratio of the protonated form was increased (Fig. 15).

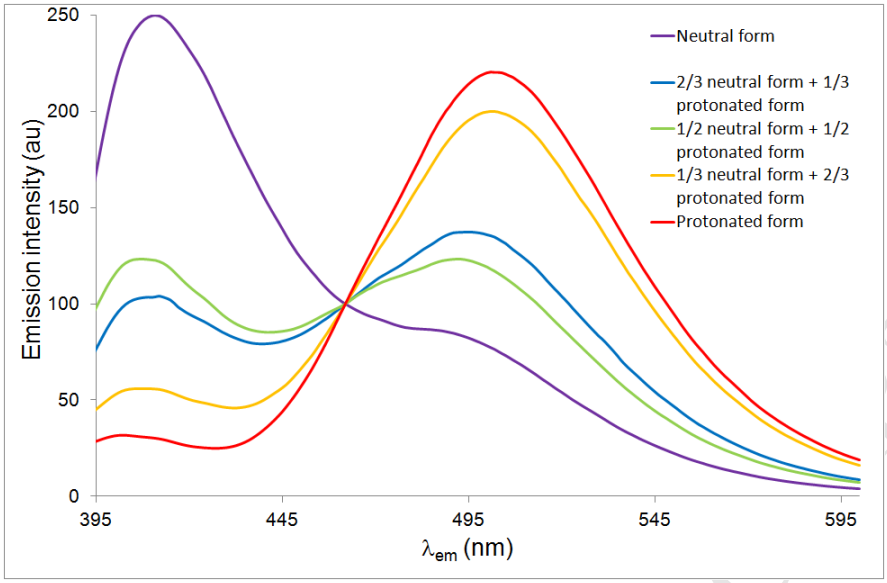

Fig. 14 Emission spectra of thin films of polystyrene doped with 1% wt of different ratios of **1** and **8**, λ_{exc} = 380 nm.

Table 7 CIE coordinates of thin films of polystyrene doped with 1 %wt of various ratios of **1**/**8**, λ_{exc} = 380 nm.

1/**8** ratio	Chromaticity coordinates (x,y)
1/0	(0.16, 0.13)
2/1	(0.16, 0.27)
1/1	(0.18, 0.24)
1/2	(0.17, 0.38)
0/1	(0.17, 0.41)

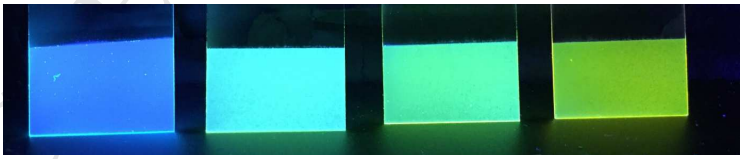

Fig. 15 Colors of polystyrene thin films doped with **7** (1 wt%) in the absence and the presence of 0.4, 0.6, and 5 equiv of TFA (from left to right). Photographs were taken in the dark upon irradiation with a hand-held UV lamp (λ_{em} = 366 nm).

Conclusions

In summary, the thermal, electrochemical, and optical properties of several TPA push-pull chromophores were studied. Both the influence of branching (dipolar, quadrupolar and tripodal structures) and the nature of the π-linker were thoroughly considered. The materials could be easily protonated with TFA at the nitrogen atom of the pyridine ring and the corresponding trifluoroacetate salts were isolated and characterized. Due to the higher electron-withdrawing character of the pyridinium ring when compared to the pyridine ring, the protonation of these chromophores resulted in an enhanced ICT into the molecule. As a consequence, the pyridinium salts exhibited a red-shifted emission band. The controlled protonation of the blue emitting pyridine derivatives led to white photoluminescence by formation of a yellow/orange emissive pyridinium form. In solid state, multi-color photoluminescence of doped polystyrene thin films was also achieved by tuning the ratio of the pyridine/pyridinium forms. This phenomenon opens up the opportunity of exploiting these materials for the fabrication multi-color OLEDs after suitable design of the molecules. The electroluminescence properties of these chromophores are currently under investigation.

Experimental section

General

Details concerning material and methods are provided in the ESI. Synthesis and full spectroscopic characterization of previously known target chromophores **1**, **3**, **6**, and **7** is given in the ESI.

General procedure for Suzuki–Miyaura cross-coupling (chromophores 1–3)

The appropriate mono-, di- or tri-iodo TPA derivative (300 mg) and pyridin-4-ylboronic acid were dissolved in a mixture of dioxane/H_2O (25 mL, 4/1). Ar was bubbled through the

mixture for 10 min and [$PdCl_2(PPh_3)_2$], Na_2CO_3 and PPh_3 were added. The reaction mixture was stirred at 90 °C for 12 h. The cooled reaction mixture was diluted with H_2O (50 mL) and extracted with CH_2Cl_2 (2 × 50 mL). The combined organic extracts were then washed with brine and dried (Na_2SO_4). Finally, the solvents were evaporated under vacuum and the crude product was purified by column chromatography (SiO_2, appropriate eluent).

Chromophore 2. The title compound was synthesized from 4,4'-diiodotriphenylamine (300 mg, 0.604 mmol), pyridin-4-ylboronic acid (163 mg, 1.328 mmol), [$PdCl_2(PPh_3)_2$] (16.95 mg, 0.024 mmol), Na_2CO_3 (128 mg, 1.207 mmol) and PPh_3 (6.33 mg, 0.024 mmol) following the general procedure for Suzuki–Miyaura cross-coupling. Orange solid. Yield: 219 mg (91%). R_f: 0.25 (SiO_2, EtOAc/MeOH 10/1). Mp: 147 °C. ^{1}H NMR (500 MHz, $CDCl_3$): δ (ppm) 7.11 (t, 1H, ^3J = 7.5 Hz, CH_{Ar}), 7.16–7.19 (m, 6H, CH_{Ar}), 7.31 (t, 2H, ^3J = 7.5 Hz, CH_{Ar}), 7.45 (d, 4H, ^3J = 5.5 Hz, CH_{Py}), 7.53 (d, 4H, ^3J = 9.0 Hz, CH_{Ar}), 8.60 (d, 4H, ^3J = 5.5 Hz, CH_{Py}). ^{13}C NMR (125 MHz, $CDCl_3$): δ (ppm) 121.0, 124.0, 124.4, 125.6, 127.9, 129.8, 132.1, 146.9, 147.5, 148.4, 150.4. HR-MALDI-MS (DHB): calcd for $C_{28}H_{21}N_3$ (M^+) 399.1730, found 399.1737.

General procedure for Sonogashira cross-coupling (chromophores 4–6)

The appropriate mono-, di- or tri-acetylene TPA derivative (200 mg) and 4-iodopyridine were dissolved in a mixture of dioxane/piperidine (25 mL, 4/1). Ar was bubbled through the mixture for 10 min and [$Pd(PPh_3)_4$] and CuI were added. The reaction mixture was stirred at 90 °C for 12 h. The cooled reaction mixture was diluted with H_2O (50 mL) and extracted with CH_2Cl_2 (2 × 50 mL). The combined organic extracts were then washed with saturated NH_4Cl solution, brine, and dried. Finally, the solvents were evaporated under vacuum and the crude product was purified by column chromatography (SiO_2, appropriate eluent).

Chromophore 4. The title compound was synthesized from 4-ethynyltriphenylamine (200 mg, 0.743 mmol), 4-iodopyridine (167 mg, 0.817 mmol), [$Pd(PPh_3)_4$] (17.16 mg, 0.015

mmol) and CuI (2.83 mg, 0.015 mmol) following the general procedure for Sonogashira cross-coupling. Yellow solid. Yield: 231 mg (90%). R_f: 0.6 (SiO_2, $CHCl_3$/EtOAc 1/1). Mp: 196–197 °C. ^{1}H NMR (500 MHz, $CDCl_3$): δ (ppm) 7.00 (d, 2H, ^3J = 8.5 Hz, CH_{Ar}), 7.08 (t, 2H, ^3J = 7.5 Hz, CH_{Ar}), 7.12 (d, 4H, ^3J = 7.5 Hz, CH_{Ar}), 7.28 (t, 4H, ^3J = 7.5 Hz, CH_{Ar}), 7.33 (d, 2H, ^3J = 5.5 Hz, CH_{Py}), 7.37 (d, 2H, ^3J = 8.5 Hz, CH_{Ar}), 8.56 (d, 2H, ^3J = 5.5 Hz, CH_{Py}). ^{13}C NMR (125 MHz, $CDCl_3$): δ (ppm) 86.2, 94.9, 114.4, 121.8, 124.1, 125.4, 125.5, 129.7, 132.0, 133.1, 147.1, 148.9, 149.9. HR-MALDI-MS (DHB): calcd for $C_{25}H_{18}N_2$ (M^+) 346.1465, found 346.1473.

Chromophore 5. The title compound was synthesized from 4,4'-diethynyltriphenylamine (200 mg, 0.682 mmol), 4-iodopyridine (307 mg, 1.5 mmol), [$Pd(PPh_3)_4$] (31.51 mg, 0.027 mmol) and CuI (5.19 mg, 0.027 mmol) following the general procedure for Sonogashira cross-coupling. Yellow solid. Yield: 265 mg (87%). R_f: 0.6 (SiO_2, EtOAc/MeOH 10/1). Mp: 118 °C. ^{1}H NMR (500 MHz, $CDCl_3$): δ (ppm) 7.05 (d, 4H, ^3J = 8.5 Hz, CH_{Ar}), 7.12–7.15 (m, 3H, CH_{Ar}), 7.30–7.31 (m, 2H, CH_{Ar}), 7.34 (d, 4H, ^3J = 6.0 Hz, CH_{Py}), 7.41 (d, 4H, ^3J = 8.5 Hz, CH_{Ar}), 8.56 (d, 4H, ^3J = 6.0 Hz, CH_{Py}). ^{13}C NMR (125 MHz, $CDCl_3$): δ (ppm) 86.6, 94.3, 116.0, 123.3, 124.9, 125.6, 126.1, 129.9, 131.8, 133.2, 146.4, 148.0, 149.9. HR-MALDI-MS (DHB): calcd for $C_{32}H_{21}N_3$ (M^+) 447.1730, found 447.1739.

General procedure for the synthesis of pyridinium salts

The appropriate chromophore **1**–**7** (100 mg) was dissolved in chloroform (2 mL) and TFA (50 µl) was added dropwise. The solution was cooled to –10 °C and the pyridinium salt was precipitated by gradual addition of cold pentane. The solid was collected by filtration and washed several times with pentane.

Chromophore 8. The title compound was synthesized from **1** (100 mg, 0.31 mmol) following the general procedure for pyridinium salts. Yellow solid. Yield: 112 mg (83%). Mp: 115 °C. ^{1}H NMR (500 MHz, $CDCl_3$): δ (ppm) 7.11 (d, 2H, ^3J = 9.0 Hz, CH_{Ar}), 7.15–7.18 (m, 6H,

CH_{Ar}), 7.33–7.36 (m, 4H, CH_{Ar}), 7.60 (d, 2H, ^{3}J = 9.0 Hz, CH_{Ar}), 7.88 (d, 2H, ^{3}J = 6.5 Hz, CH_{Py}), 8.72 (d, 2H, ^{3}J = 6.5 Hz, CH_{Py}). ^{13}C NMR (125 MHz, $CDCl_3$): δ (ppm) 116.9 (q, $^{1}J_{CF}$ = 290 Hz), 121.2, 122.1, 125.2, 125.9, 126.2, 128.7, 130.0, 142.2, 146.4, 151.7, 155.5, 163.0 (q, $^{2}J_{CF}$ = 38 Hz). HR-MALDI-MS (no matrix): calcd for $C_{23}H_{18}N_2$ $[(M - C_2F_3O_2H)^+]$ 322.1465, found 322.1469.

Chromophore 9. The title compound was synthesized from **2** (100 mg, 0.25 mmol) following the general procedure for pyridinium salts. Orange solid. Yield: 139 mg (89%). Mp: 133 °C. ^{1}H NMR (500 MHz, $CDCl_3$): δ (ppm) 7.21 (d, 2H, ^{3}J = 7.5 Hz, CH_{Ar}), 7.26–7.29 (m, 5H, CH_{Ar}), 7.42 (t, 2H, ^{3}J = 7.5 Hz, CH_{Ar}), 7.68 (d, 4H, ^{3}J = 9.0 Hz, CH_{Ar}), 7.92 (d, 4H, ^{3}J = 6.5 Hz, CH_{Py}), 8.80 (d, 4H, ^{3}J = 6.5 Hz, CH_{Py}), 11.09 (br s, 2H, NH). ^{13}C NMR (125 MHz, $CDCl_3$); δ (ppm) 122.7, 124.0, 126.4, 126.9, 128.9, 129.0, 130.4, 142.9, 145.7, 150.1, 154.9, 162.9 (q, $^{2}J_{CF}$ = 38 Hz). HR-MALDI-MS (no matrix): calcd for $C_{28}H_{21}N_3$ $[(M - C_4F_6O_4H_2)^+]$ 399.1730, found 399.1738.

Chromophore 10. The title compound was synthesized from **3** (100 mg, 0.21 mmol) following the general procedure for pyridinium salts. Orange solid. Yield: 160 mg (93%). Mp: 196 °C. ^{1}H NMR (500 MHz, $CDCl_3$): δ (ppm) 2.85 (br s, 3H, NH), 7.37 (d, 6H, ^{3}J = 8.5 Hz, CH_{Ar}), 7.75 (d, 6H, ^{3}J = 8.5 Hz, CH_{Ar}), 7.94 (d, 6H, ^{3}J = 6.0 Hz, CH_{Py}), 8.85 (d, 6H, ^{3}J = 6.0 Hz, CH_{Py}). ^{13}C NMR (125 MHz, $CDCl_3$): δ (ppm) 122.1, 125.1, 128.9, 132.0, 146.9, 148.6, 151.0. HR-MALDI-MS (no matrix): calcd for $C_{33}H_{24}N_4$ $[(M - C_6F_9O_6H_3)^+]$ 476.1995, found 476.2003.

Chromophore 11. The title compound was synthesized from **4** (100 mg, 0.29 mmol) following the general procedure for pyridinium salts. Yellow solid. Yield: 117 mg (88%). Mp: 141 °C. ^{1}H NMR (500 MHz, $CDCl_3$): δ (ppm) 6.99 (d, 2H, ^{3}J = 8.5 Hz, CH_{Ar}), 7.12–7.15 (m, 6H, CH_{Ar}), 7.32 (t, 4H, ^{3}J = 7.5 Hz, CH_{Ar}), 7.40 (d, 2H, ^{3}J = 8.5 Hz, CH_{Ar}), 7.71 (d, 2H, ^{3}J = 6.0 Hz, CH_{Py}), 8.70 (d, 2H, ^{3}J = 6.0, CH_{Py}), 10.59 (br s, 1H, NH). ^{13}C NMR (125 MHz

$CDCl_3$): δ (ppm) 85.7, 104.0, 111.9, 116.6 (q, $^1J_{CF}$ = 288 Hz), 120.7, 124.9, 126.1, 127.5, 129.9, 133.9, 140.1, 142.7, 146.5, 150.4, 162.7 (q, $^2J_{CF}$ = 38 Hz). HR-MALDI-MS (DHB): calcd for $C_{25}H_{18}N_2$ [$(M - C_2F_3O_2H)^+$] 346.1465, found 346.1468.

Chromophore 12. The title compound was synthesized from **5** (100 mg, 0.22 mmol) following the general procedure for pyridinium salts. Yellow solid. Yield 141 mg (95%). Mp: 192 °C (decomposition). ^{1}H NMR (500 MHz, $CDCl_3$): δ (ppm) 3.82 (br s, 2H, NH), 7.10 (d, 4H, ^3J = 8.5 Hz, CH_{Ar}), 7.16 (d, 2H, ^3J = 8.0 Hz, CH_{Ar}), 7.21–7.23 (m, 1H, CH_{Ar}), 7.38 (t, 2H, ^3J = 8.0 Hz, CH_{Ar}), 7.48 (d, 4H, ^3J = 8.5 Hz, CH_{Ar}), 7.72 (d, 4H, ^3J = 6.0 Hz, CH_{Py}), 8.73 (d, 4H, ^3J = 6.0 Hz, CH_{Py}). ^{13}C NMR (125 MHz, $CDCl_3$): δ (ppm) 85.9, 102.5, 114.5, 116.4 (q, $^1J_{CF}$ = 288 Hz), 123.2, 126.1, 126.8, 127.7, 130.3, 134.1, 139.6, 143.0, 145.8, 149.1, 162.4 (q, $^2J_{CF}$ = 38 Hz). HR-MALDI-MS (DHB): calcd for $C_{32}H_{21}N_3$ [$(M - C_4F_6O_4H_2)^+$] 447.1730, found 447.1735.

Chromophore 13. The title compound was synthesized from **6** (100 mg, 0.18 mmol) following the general procedure for pyridinium salts. Orange solid. Yield 152 mg (95%). Mp: 199 °C (decomposition). ^{1}H NMR (500 MHz, $CDCl_3$): δ (ppm) 7.17 (d, 6H, ^3J = 8.5 Hz, CH_{Ar}), 7.56 (d, 6H, ^3J = 8.5 Hz, CH_{Ar}), 7.80 (d, 6H, ^3J = 6.0 Hz, CH_{Py}), 8.80 (d, 6H, ^3J = 6.0 Hz, CH_{Py}). ^{13}C NMR (125 MHz, $CDCl_3$): δ (ppm) 86.1, 102.5, 116.0, 116.3 (q, $^1J_{CF}$ = 288 Hz), 124.6, 128.1, 134.4, 140.2, 142.5, 148.2, 162.2 (q, $^2J_{CF}$ = 38 Hz). HR-MALDI-MS (DHB): calcd for $C_{39}H_{27}N_4$ [$(M - C_6F_9O_6)^+$] 551.2214, found 551.2223.

Chromophore 14. The title compound was synthesized from **7** (100 mg, 0.29 mmol) following the general procedure for pyridinium salts. Red solid. Yield 125 mg (93%). Mp: 189 °C. ^{1}H NMR (500 MHz, $CDCl_3$): δ (ppm) 6.95 (d, 1H, ^3J = 16.0 Hz, CH_{vin}), 7.03 (d, 2H, ^3J = 8.5 Hz, CH_{Ar}), 7.12–7.16 (m, 6H, CH_{Ar}), 7.30–7.34 (m, 4H, CH_{Ar}), 7.44 (d, 2H, ^3J = 8.5 Hz, CH_{Ar}), 7.54 (d, 1H, ^3J = 16.0 Hz, CH_{vin}), 7.77 (d, 2H, ^3J = 6.5 Hz, CH_{Py}), 8.67 (d, 2H, ^3J = 6.5 Hz, CH_{Py}). ^{13}C NMR (125 MHz, $CDCl_3$): δ (ppm) 116.1 (q, $^1J_{CF}$ = 286 Hz), 119.5,

121.2, 122.4, 126.0, 127.1, 129.7, 129.9, 141.2, 141.3, 146.6, 150.9, 154.8, 161.8 (q, $^{2}J_{CF}$ = 38 Hz). HR-MALDI-MS (DHB): calcd for $C_{25}H_{21}N_2$ [$(M - C_2F_3O_2)^+$] 349.1694, found 349.1699.

Electronic supplementary information (ESI) available: Experimental procedures, copies of the ^{1}H NMR and ^{13}C NMR spectra of the new compounds, DSC thermographs, cyclic voltammograms, crystallographic data, crystal structures, visualization of HOMO/LUMO localizations, UV and PL spectra. Crystallographic data for structural analysis have been deposited in the Cambridge Crystallographic Data Centre, CCDC no. 1522362, 1522363, 1522364 and 1522365 for **1**, **2**, **3**, and **10**, respectively. Copies of this information may be obtained free of charge from The Director, CCDC, 12 Union Road, Cambridge CB2 1EY, UK (fax: +44-1223-336033; e-mail: deposit@ccdc.cam.ac.uk or www: http://www.ccdc.cam.ac.uk).

Acknowledgements

This research was supported by the Technology Agency of the Czech Republic (TE01020022, Flexprint).

References

1 Z. Wu and D. Ma, *Mat. Sci. Eng. R*, 2016, **107**, 1–42.

2 S. Mukherjee and P. Thilagar, *Dyes Pigm.*, 2014, **110**, 2–27.

3 J. Kido, K. Hongawa, K. Okuyama and K. Nagai, *Appl. Phys. Lett.*, 1994, **64**, 815–817.

4 J. Kido, M. Kimura and K. Nagai, *Science*, 1995, **267**, 1332–4.

5 H. Klauk, Ed., *Organic Electronics: Materials, Manufacturing and Applications*, Wiley-VCH, 2006.

6 Z. Li, Z. R. Li and H. Meng, Eds., *Organic Light-Emitting Materials and Devices*, Taylor & Francis, 2006.

7 T. Tsujimura, *OLED Displays: Fundamentals and Applications*, Wiley, 2012.

8 T. Jeon, B. Geffroy, D. Tondelier, Y. Bonnassieux, S. Forget, S. Chenais and E. Ishow, *Thin Solid Films*, 2013, **542**, 263–269.

9 S. Tao, Y. Zhou, C.-S. Lee, S.-T. Lee, D. Huang and X. Zhang, *J. Mater. Chem.*, 2008, **18**, 3981–3984.

10 T. Fleetham, J. Ecton, Z. Wang, N. Bakken and J. Li, *Adv. Mater.*, 2013, **25**, 2573–2576.

11 E. Angioni, M. Chapran, K. Ivaniuk, N. Kostiv, V. Cherpak, P. Stakhira, A. Lazauskas, S. Tamulevičius, D. Volyniuk, N. J. Findlay, T. Tuttle, J. V Grazulevicius and P. J. Skabara, *J. Mater. Chem. C*, 2016, **4**, 3851–3856.

12 D. Liu, Z. Zhang, H. Zhang and Y. Wang, *Chem. Commun.*, 2013, **49**, 10001–10003.

13 H. V Huynh, X. He and T. Baumgartner, *Chem. Commun.*, 2013, **49**, 4899–4901.

14 C. Romero-Nieto, S. Durben, I. M. Kormos and T. Baumgartner, *Adv. Funct. Mater.*, 2009, **19**, 3625–3631.

15 Y. Yang, M. Lowry, C. M. Schowalter, S. O. Fakayode, J. O. Escobedo, X. Xu, H. Zhang, T. J. Jensen, F. R. Fronczek, I. M. Warner and R. M. Strongin, *J. Am. Chem. Soc.*, 2006, **128**, 14081–14092.

16 K. Yamaguchi, T. Murai, J. Guo, T. Sasamori and N. Tokitoh, *Chem. Open*, 2016, **5**, 434–438.

17 U. Giovanella, E. Cariati, E. Lucenti, M. Pasini, F. Galeotti and C. Botta, *ChemPhysChem*, 2017, doi: 10.1002/cphc.201700185

18 Y. Shiraishi, C. Ichimura, S. Sumiya and T. Hirai, *Chem. - Eur. J.*, 2011, **17**, 8324–8332.

19 G. Bordeau, R. Lartia, G. Metge, C. Fiorini-Debuisschert, F. Charra and M. P. Teulade-Fichou, *J. Am. Chem. Soc.*, 2008, **130**, 16836–16837.

20 A. Bhaskar, G. Ramakrishna, Z. Lu, R. Twieg, J. M. Hales, D. J. Hagan, E. Van

Stryland and T. Goodson, *J. Am. Chem. Soc.*, 2006, **128**, 11840–11849.

21 S. Sonu, A. K. Tiwari, A. Sarmah, R. K. Roy and S. K. Saha, *Dyes Pigm.*, 2014, **102**, 114–125.

22 S. Achelle, I. Nouira, B. Pfaffinger, Y. Ramondenc, N. Plé and J. Rodríguez-López, *J. Org. Chem.*, 2009, **74**, 3711–3717.

23 S. Kato, Y. Yamada, H. Hiyoshi, K. Umezu and Y. Nakamura, *J. Org. Chem.*, 2015, **80**, 9076–9090.

24 E. V. Verbitskiy, A. A. Baranova, K. I. Lugovik, K. O. Khokhlov, E. M. Cheprakova, M. Z. Shafikov, G. L. Rusinov, O. N. Chupakhin and V. N. Charushin, *Dyes. Pigm.*, 2017, **137**, 360–371.

25 S. Achelle, A. Barsella, B. Caroa and F. Robin-le Guen, *RSC Adv.*, 2015, **5**, 39218–39227.

26 V. Schmitt, S. Mosche and H. Detert, *Eur. J. Org. Chem.*, 2013, 5655–5669.

27 K. Hoffert, R. Durand, S. Gauthier, F. Robin-le Guen and S. Achelle, *Eur. J. Org. Chem.*, 2017, 523-529.

28 S. Achelle, J. Rodríguez-López and F. Robin-le Guen, *J. Org. Chem.*, 2014, **79**, 7564–71.

29 C. A. B. Rodrigues, I. F. A. Mariz, E. M. S. Maçôas, C. A. M. Afonso and J. M. G. Martinho, *Dyes Pigm.*, 2013, **99**, 642–652.

30 R. Tang, X. Wang, W. Zhang, X. Zhuang, S. Bi, W. Zhang and F. Zhang, *J. Mater. Chem. C*, 2016, **4**, 7640–7648.

31 E. Cariati, C. Dragonetti, E. Lucenti, F. Nisic, S. Righetto, D. Roberto and E. Tordin, *Chem. Commun.*, 2014, **50**, 1608–1610.

32 S. Achelle, L. Bodiou, J. Charrier and F. Robin-le Guen, *C. R. Chim.*, 2016, **19**, 279–285.

33 K. Melánová, D. Cvejn, F. Bureš, V. Zima, J. Svoboda, L. Beneš, T. Mikysek, O. Pytela and P. Knotek, *Dalton Trans.*, 2014, **43**, 10462–10470.

34 C. Hadad, S. Achelle, I. López-Solera, J. C. García-Martínez and J. Rodríguez-López, *Dyes Pigm.*, 2013, **97**, 230–237.

35 S. Achelle, J. Rodríguez-López, F. Bureš and F. Robin-le Guen, *Dyes Pigm.*, 2015, **121**, 305–311.

36 S. Achelle, S. Kahlal, A. Barsella, J. Y. Saillard, X. Che, J. Vallet, F. Bureš, B. Caro and F. Robin-le Guen, *Dyes Pigm.*, 2015, **113**, 562–570.

37 B. Dumat, G. Bordeau, E. Faurel-Paul, F. Mahuteau-Betzer, N. Saettel, G. Metge, C. Fiorini-Debuisschert, F. Charra and M. P. Teulade-Fichou, *J. Am. Chem. Soc.*, 2013, **135**, 12697–12706.

38 S. Achelle, J. Rodríguez-López, N. Cabon and F. Robin-le Guen, *RSC Adv.*, 2015, **5**,

107396–107399.

39 S. Achelle, J. Rodríguez-López, C. Katan and F. Robin-le Guen, *J. Phys. Chem C*, 2016, **120**, 26986–26995.

40 L. Wenfeng, M. Hengchang, L. Con, M. Yuan, Q. Chunxuan, Z. Zhonwei, Y. Zengming, C. Haiying and L. Ziqiang, *RSC Adv.*, 2015, **5**, 6869–6878.

41 W. Shi, F. Ma and Z. Xie, *Sensors Actuators B Chem.*, 2015, **220**, 600–606.

42 W. Shi, S. Zhao, Y. Su, Y. Hui, Z. Xie, W. Shi, S. Zhao, Y. Su, Y. Hui and Z. Xie, *New J. Chem.*, 2016, **40**, 7814–7820.

43 P. B. Pati and S. S. Zade, *Eur. J. Org. Chem.*, 2012, 6555–6561.

44 Q. Zhang, J. Zhang, H. Zuo, C. Wang and Y. Shen, *Tetrahedron*, 2016, **72**, 1244–1248.

45 X. Yang, X. Chen, X. Lu, C. Yan, Y. Xu, X. Hang, J. Qu and R. Liu, *J. Mater. Chem. C*, 2016, **4**, 383–390.

46 L. Wang, L. Yang, L. Li and D. Cao, *New J. Chem.*, 2016, **40**, 6706–6713.

47 M. Hengchang, Z. Zhongwei, J. Yuanyuan, Z. Lajia, Q. Chunxuan, C. Haiying, Y. Zengming, Y. Zhiwanga and L. Ziqiang, *RSC Adv.*, 2015, **5**, 87157–87167.

48 A. Chowdhury and P. S. Mukherjee, *J. Org. Chem.*, 2015, **80**, 4064–4075.

49 G. Vamvounis, P. E. Shaw and P. L. Burn, *J. Mater. Chem. C*, 2013, **1**, 1322–1329.

50 E. V. Verbitskiy, A. A. Baranova, K. I. Lugovik, M. Z. Shafikov, K. O. Khokhlov, E. M. Cheprakova, G. L. Rusinov, O. N. Chupakhin and V. N. Charushin, *Anal. Bioanal. Chem.*, 2016, **408**, 4093–4101.

51 D. Cvejn, E. Michail, K. Seintis, M. Klikar, O. Pytela, T. Mikysek, N. Almonasy, M. Ludwig, V. Giannetas, M. Fakis and F. Bureš, *RSC Adv.*, 2016, **6**, 12819–12828.

52 D. Cvejn, S. Achelle, O. Pytela, J. P. Malval, A. Spangenberg, N. Cabon, F. Bureš and F. Robin-le Guen, *Dyes Pigm.*, 2016, **124**, 101–109.

53 P. Hrobárik, V. Hrobáriková, I. Sigmundová, P. Zahradník, M. Fakis, I. Polyzos and P. Persephonis, *J. Org. Chem.*, 2011, **76**, 8726–8736.

54 C. Katan, F. Terenziani, O. Mongin, M. H. V Werts, L. Porrès, T. Pons, J. Mertz, S. Tretiak and M. Blanchard-Desce, *J. Phys. Chem. A*, 2005, **109**, 3024–3037.

55 L. Porrès, O. Mongin, C. Katan, M. Charlot, T. Pons, J. Mertz and M. Blanchard-Desce, *Org. Lett.*, 2004, **6**, 47–50.

56 V. Parthasarathy, S. Fery-Forgues, E. Campioli, G. Recher, F. Terenziani and M. Blanchard-Desce, *Small*, 2011, **7**, 3219–3229.

57 C. Le Droumaguet, A. Sourdon, E. Genin, O. Mongin and M. Blanchard-Desce, *Chem. - Asian J.*, 2013, **8**, 2984–3001.

58 B. Dumat, G. Bordeau, A. I. Aranda, F. Mahuteau-Betzer, Y. El Harfouch, G. Metgé, F. Charra, C. Fiorini-Debuisschert and M.-P. Teulade-Fichou, *Org. Biomol. Chem.*,

2012, **10**, 6054–6061.

59 R. Lartia, C. Allain, G. Bordeau, F. Schmidt, C. Fiorini-Debuisschert, F. Charra and M. P. Teulade-Fichou, *J. Org. Chem.*, 2008, **73**, 1732–1744.

60 W. Yang, C. Li, M. Zhang, W. Zhou, R. Xue, H. Liu and Y. Li, *Phys. Chem. Chem. Phys.*, 2016, **18**, 28052–28060.

61 Z.-F. Chang, L.-M. Jing, Y.-Y. Liu, J.-J. Liu, Y.-C. Ye, Y. S. Zhao, S.-C. Yuan and J.-L. Wang, *J. Mater. Chem. C*, 2016, **4**, 8407–8415.

62 Z. Li, T. Ye, S. Tang, C. Wang, D. Ma and Z. Li, *J. Mater. Chem. C*, 2015, **3**, 2016–2023.

63 M. C. Tang, C. K. M. Chan, D. P. K. Tsang, Y. C. Wong, M. M. Y. Chan, K. M. C. Wong and V. W. W. Yam, *Chem. - Eur. J.*, 2014, **20**, 15233–15241.

64 X. Han, Q. Bai, L. Yao, H. Liu, Y. Gao, J. Li, L. Liu, Y. Liu, X. Li, P. Lu and B. Yang, *Adv. Funct. Mater.*, 2015, **25**, 7521–7529.

65 C. Allain, F. Schmidt, R. Lartia, G. Bordeau, C. Fiorini-Debuisschert, F. Charra, P. Tauc and M. P. Teulade-Fichou, *ChemBioChem*, 2007, **8**, 424–433.

66 C. W. Bird, *Tetrahedron*, 1986, **42**, 89–92.

67 S. I. Kotelevskii and O. V. Prezhdo, *Tetrahedron*, 2001, **57**, 5715–5729.

68 T. M. Krygowski, H. Szatylowicz, O. A. Stasyuk, J. Dominikowska and M. Palusiak, *Chem. Rev.*, 2014, **114**, 6383–6422.

69 F. Bureš, D. Cvejn, K. Melánová, L. Beneš, J. Svoboda, V. Zima, O. Pytela, T. Mikysek, Z. Růžičková, I. V. Kityk, A. Wojciechowski and N. AlZayed, *J. Mater. Chem. C*, 2016, **4**, 468–478.

70 M. Klikar, I. V. Kityk, D. Kulwas, T. Mikysek, O. Pytela and F. Bureš, *New J. Chem.*, 2017, **41**, 1459–1472.

71 D. Cvejn, E. Michail, I. Polyzos, N. Almonasy, O. Pytela, M. Klikar, T. Mikysek, V. Giannetas, M. Fakis and F. Bureš, *J. Mater. Chem. C*, 2015, **3**, 7345–7355.

72 M. J. Frisch, G. W. Trucks, H. B. Schlegel, G. E. Scuseria, M. A. Robb, J. R. Cheeseman, G. Scalmani, V. Barone, B. Mennucci, G. A. Petersson, H. Nakatsuji, M. Caricato, X. Li, H. P. Hratchian, A. F. Izmaylov, J. Bloino, G. Zheng, J. L. Sonnenberg, M. Hada, M. Ehara, K. Toyota, R. Fukuda, J. Hasegawa, M. Ishida, T. Nakajima, Y. Honda, O. Kitao, H. Nakai, T. Vreven, J. A. Montgomery, Jr., J. E. Peralta, F. Ogliaro, M. Bearpark, J. J. Heyd, E. Brothers, K. N. Kudin, V. N. Staroverov, T. Keith, R. Kobayashi, J. Normand, K. Raghavachari, A. Rendell, J. C. Burant, S. S. Iyengar, J. Tomasi, M. Cossi, N. Rega, J. M. Millam, M. Klene, J. E. Knox, J. B. Cross, V. Bakken, C. Adamo, J. Jaramillo, R. Gomperts, R. E. Stratmann, O. Yazyev, A. J. Austin, R. Cammi, C. Pomelli, J. W. Ochterski, R. L. Martin, K. Morokuma, V. G. Zakrzewski, G. A. Voth, P. Salvador, J. J. Dannenberg, S. Dapprich, A. D. Daniels, O. Farkas, J. B. Foresman, J. V. Ortiz, J. Cioslowski and D. J. Fox, Gaussian 09, Revision D.01, Gaussian, Inc, Wallingford CT, 2013.

73 S. Easwaramoorthi, P. Thamaraiselvi, K. Duraimurugan, A. J. Beneto, A. Siva and B. U. Nair, *Chem. Commun.*, 2014, **50**, 6902–6905.

74 C. Reichardt, *Chem. Rev.*, 1994, **94**, 2319–2358.

75 J. P. Cerón-Carrasco, D. Jacquemin, C. Laurence, A. Planchat, C. Reichardt and K. Sraïdi, *J. Phys. Org. Chem.*, 2014, **27**, 512–518.

76 Z. Otwinowski and W. Minor, *Methods Enzymol*. 1997, **276**, 307-326.

77 P. Coppens In: F.R. Ahmed, S.R. Hall, C.P. Huber Editors, Crystallographic Computing, **1970**, pp. 255 – 270, Copenhagen, Munksgaard.

78 A. Altomare, G. Cascarano, C. Giacovazzo and A. Guagliardi, *J. Appl.Cryst.* 1994, **27**, 1045-1050.

79 G. M. Sheldrick, SHELXL-97, University of Göttingen: Göttingen, **2008.**

80 G. M. Sheldrick, *Acta Cryst.* 2015, C71, 3-8.

Triphenylamines bearing pyridine(s) and their trifluoroacetate salts are described

Increase in the intramolecular charge transfer is observed upon protonation

White photoluminescence was obtained in solution by the controlled protonation